remote sensing

MDPI

Article

Cost-Efficient Multi-GNSS Station with Real-Time Transmission for Geodynamics Applications

Maurin Vidal [1], Paul Jarrin [1,*], Lucie Rolland [1], Jean-Mathieu Nocquet [1,2], Mathilde Vergnolle [1] and Pierre Sakic [2]

[1] Université Côte d'Azur, CNRS, IRD, Observatoire de la Côte d'Azur, Géoazur, 06560 Valbonne, France; maurin.vidal@geoazur.unice.fr (M.V.); lucie.rolland@geoazur.unice.fr (L.R.); nocquet@geoazur.unice.fr (J.-M.N.); mathilde.vergnolle@geoazur.unice.fr (M.V.)
[2] Institut de Physique du Globe de Paris, Université Paris Cité, 75005 Paris, France; sakic@ipgp.fr
* Correspondence: paul.jarrin@geoazur.unice.fr

Abstract: GNSS is a standard tool for monitoring and studying the Earth's dynamic environment. However, the development of dense GNSS measurements remains limited in many experiments by the cost of high-class geodetic equipment to achieve the high precision required by many applications. Recently, multi-constellation, multi-frequency, low-power and, above all, less expensive GNSS electronic chips have become available. We present a prototype of a low-cost, open-source multi-GNSS station. Our prototype comprises a dual-frequency GNSS chip, a calibrated antenna, a Raspberry Pi card and a 4G key for data transmission. The system is easy to deploy in the field and allows precise positioning in real-time and post-processing. We assess the performance of our prototype in terms of raw data quality, and quality of the obtained high rate and daily position one-year-long time series. Our results demonstrate a quality equivalent to high-class geodetic equipment and better quality than other low-cost systems proposed so far.

Keywords: low-cost; GNSS; crustal deformation; geodynamics

Citation: Vidal, M.; Jarrin, P.; Rolland, L.; Nocquet, J.-M.; Vergnolle, M.; Sakic, P. Cost-Efficient Multi-GNSS Station with Real-Time Transmission for Geodynamics Applications. *Remote Sens.* **2024**, *16*, 991. https://doi.org/10.3390/rs16060991

Academic Editors: Yang Yang, Andrew Dempster and Suelynn Choy

Received: 16 February 2024
Revised: 6 March 2024
Accepted: 7 March 2024
Published: 12 March 2024

1. Introduction

Over the last three decades, geodetic observations have been key for monitoring the physical parameters of the Earth's environment (see [1] for a review). Observed parameters include the motion of tectonic plates, slow crustal deformation, transient slip along faults, seismic waves during earthquakes, landslide monitoring, volcanic deformation, sea surface and moisture estimates near GNSS antennas, water content monitoring in the troposphere, monitoring of the ionosphere, in addition to the realization of reference frames that define the basis of most applications. Scientists studying earth science have made huge efforts to improve the spatial coverage of permanent Global Navigation Satellite System (GNSS) networks and to support the continuity of observation over time. Such efforts incur significant costs, due to the current price of high-class GNSS receivers and antennas and then the logistics required for installation and regular maintenance. High-class GNSS stations, through high tracking performance of the satellite signals, allow position measurements with an accuracy of one to a few millimeters for daily static positioning, which is desirable for catching and quantifying a wide range of geophysical processes. Aside from the development of permanent GNSS networks, there is also a need for affordable easy-to-deploy equipment to perform episodic GNSS measurements at geodetic markers. Survey mode measurements are useful for (1) repeated long-term surveying of tectonically active areas and (2) installing continuous temporal networks to complement the record of cos-post-seismic deformation in rapid response to large earthquakes (e.g., [1,2]).

A new approach that seems to have captured the scientific community's interest is the use of low-cost GNSS sensors, which leaves open questions about their reliability and precision regarding long-term position determination. In recent years, new cost-efficient

single- multi-frequency GNSS chips and GNSS antennas have been introduced to the commercial market (e.g., [3]). This equipment captured the scientific community's interest, possibly opening the opportunity of position solutions at a precision similar to those obtained from high-class GNSS stations. Low-cost equipment offers low energy consumption, GNSS signal to high-frequency sampling rates (up to 100 Hz in some cases) for a ∼ten to twenty times lower prices than the high-class GNSS sensors (Table 1, ∼500–1000 €). One important question for scientific applications remains to quantify the performance of such low-cost equipment and precisely assess its ability to meet the requirements of the various applications. For instance, even though single-frequency GNSS receivers can reach subcentimeter-level accuracy using short baselines and under favorable open-sky conditions [4,5], GNSS signal delays linked to the ionosphere are still the principal issue affecting their positioning solution. This is particularly true when using the Precise Point Positioning (PPP) and long baseline approaches in both static and kinematic modes (e.g., [6,7]), restricting thus the continuous surveying of several applications such as geodynamics.

Table 1. Main characteristics of the GNSS stations used in the current study. For a complete description, please refer to the respective manufacturer datasheet or the UNAVCO resources database (https://kb.unavco.org/article/unavco-resources-gnss-receivers-434.html (accessed on 10 January 2024)).

Site Name	SEPT	UBLO	SOPH	NICE
Receiver	Septentrio MOSAIC-X5	Ublox ZED-F9P	Trimble NetR9	Trimble NetR9
Antenna	ArduSimple AS-ANT3BCAL	ArduSimple AS-ANT3BCAL	Ashtech Choke ring ASH701933A_M	Trimble Zephyr 2 Geodetic
Satellite System	GPS, GLONASS, Galileo, Beidou, Navic, QZSS, SBAS	GPS, GLONASS, Galileo, Beidou, QZSS, SBAS	GPS, GLONASS, SBAS	GPS, GLONASS, Galileo, Beidou, QZSS, SBAS
Channels	448	184	440	440
Firmware upgrades	Free	Free	Not Free	Not Free
Price	∼1000 € [1]	∼500 € [1]	∼10,000 € [2]	∼10,000 € [2]

[1] Price accounts for the GNSS station + cellular modem. [2] Price should be considered as referential (local representative) and just includes the effective cost of GNSS receiver + antenna.

Previous studies have suggested a good performance of dual-frequency low-cost receivers, mainly for the u-blox ZED-F9P (https://www.u-blox.com/en/product/zed-f9p-module (accessed on 10 January 2024)) associated either with high-class or low-cost antennas, for both post- and real-time processing. Most of the published studies used GNSS observation time windows spanning from days to a few months, which might be short to assess the performance of low-cost receivers for long-term surveying ([8–12], among others). In detail, while low-cost receivers reach millimeter-level accuracy for static daily positioning, their positioning accuracy in kinematic mode appears to be more challenging when using long baselines (e.g., [9]). Recently, Tunini et al. [13] compared the performance of a u-blox ZED-F9P receiver to two high-class receivers by connecting the three receivers to the same high-class geodetic antenna. They collected five months of data in 2021 where quality check statistics showed that, for most days, the low-cost receiver retrieved 60–70% of the observations while high-class receivers retrieved 90%. Despite this drawback, the u-blox reaches a precision in daily displacement estimates comparable to the high-class geodetic receivers with a double difference post-processing strategy. Tunini et al. [13] conclude that the dual-frequency, low-cost geodetic receiver u-blox ZED-F9P, is suitable for crustal deformation studies.

In this study, we aim to improve the current state-of-the-art of low-cost GNSS receivers. In Section 2 we present a ready-to-use dual-frequency GNSS low-cost station. Our station uses a Septentrio Mosaic-X5 module (https://www.septentrio.com/en/products/gps/gnss-receiver-modules/mosaic-x5 (accessed on 10 January 2024)) and a low-cost AS-ANT3BCAL antenna (https://www.ardusimple.com/product/calibrated-survey-gnss-quadband-antenna-ip67/ (accessed on 10 January 2024)). Our GNSS station also offers data transmission capabilities through a cellular connection, making it ideal for precise post- and

real-time positioning. In Section 3 we perform a detailed analysis of a one-year-long dataset using different approaches to evaluate the quality of static and kinematic positioning for single (GPS, GLONASS, Galileo) and multi-GNSS constellations. We assess the precision by comparing the latter with respect to those obtained for high-class Trimble receivers and the low-cost u-blox receiver. Compared to previous studies using the u-blox ZED-F9P module, we find that our proposed low-cost station improves the positioning accuracy in static and kinematic modes relative to the other equipment, indicating that it is well-suited for continuous and survey-mode geophysical applications.

2. Materials and Methods

2.1. Hardware Specifications and Description of the System

The system includes a dual-frequency GNSS board associated to a Raspberry Pi B+ v1.2 card, a 4G dongle cellular modem, and an officially calibrated antenna (Figure 1). The selected GNSS chip is a mosaic-X5 (https://www.septentrio.com/en/products/gnss-receivers/receivers-module/mosaic (accessed on 10 January 2024)) GNSS receiver module from Septentrio, which has the same GNSS signal tracking capabilities as high-class GNSS receivers. The mosaic-X5 is plugged onto an electronic board (simpleRTK3B Pro) designed by ArduSimple and sold as MOSAIC-HAT (https://github.com/septentrio-gnss/mosaicHAT (accessed on 10 January 2024)). MOSAIC-HAT is an Open-source GPS/GNSS electronic board with basic communication capabilities. In order to control the MOSAIC HAT board, we plugged it into the Raspberry General Purpose Port (GPIO, Figure 2) instead of the USB port due to its robustness.

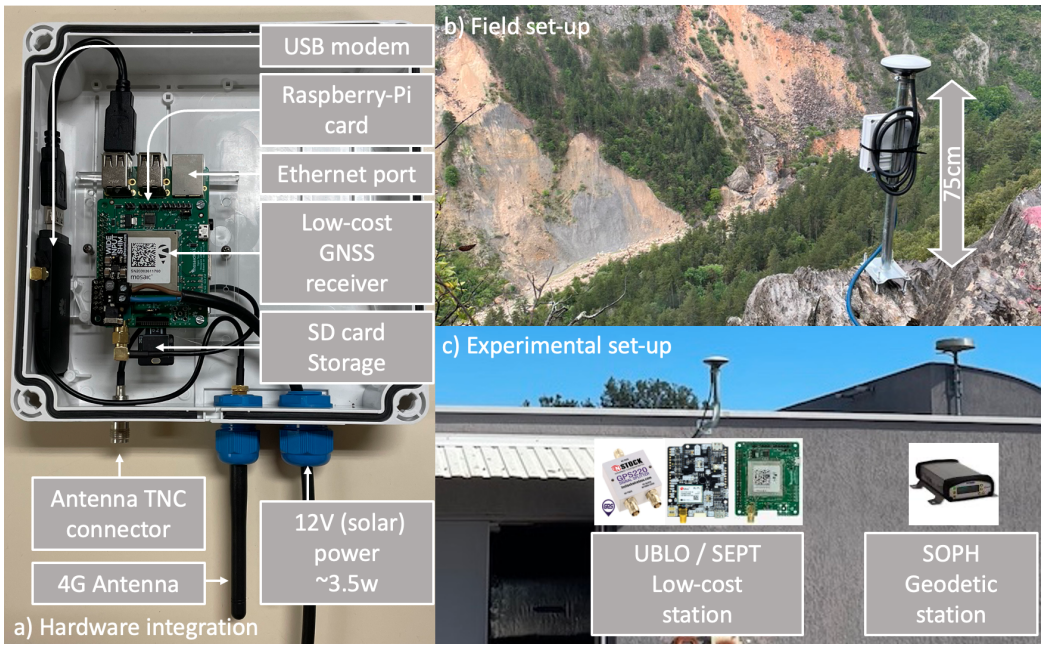

Figure 1. (**a**) The in-house cost-efficient dual-frequency low-cost receiver. (**b**) Ground-based GNSS field set-up using the Septentrio MOSAIC X5 receiver board in southern France, located ∼35 km from the SOPH station. (**c**) Experimental set-up and antenna monument, anchored into the building roof, for both the continuous GNSS SOPH station and the low-cost SEPT and UBLO stations.

The AS-ANT3BCAL (https://www.ardusimple.com/product/calibrated-survey-gnss-quadband-antenna-ip67/ (accessed on 10 January 2024)) is a triple-band GPS/GNSS antenna manufactured by Ardusimple. It is compatible with the MOSAIC-HAT board and benefits of open access calibration products provided by the National Geodetic Survey (NGS [14]) for processing geodetic observations in the International Terrestrial Reference Frame (ITRF). The antenna is rugged and relatively small in dimension (∼15 cm diameter) with respect to commonly geodetic class antennas, with Phase Center Variations (PCVs)

lower than 3 mm at all elevations [12], recommended to work in environmental conditions from −40° to +85 °C.

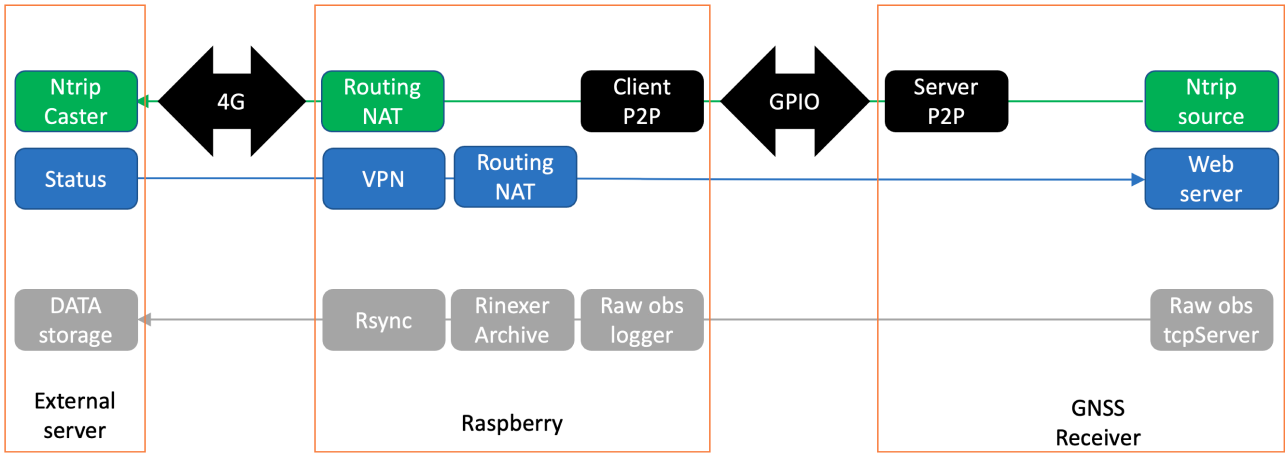

Figure 2. Flowchart implemented in Septentrio mosaic-X5 station prototype. 4G: Cellular modem. GPIO: General Purpose Port. Ntrip: Networked Transport of RTCM via Internet Protocol. VPN: Virtual Private Network. P2P: Point-two-Point. NAT: Network Address Translation.

This development aims to facilitate the deployment of GNSS stations in the field (e.g., Figure 1). It is designed for easy data transmission for either permanent networks for real-time kinematic positioning or hourly and/or daily transmission for near-real-time static positioning. It is also useful for data collection during surveys. The power consumption of the whole system, including the GNSS antenna and data transmission at a 1-s sampling rate, is ∼3.5 W. Such power consumption is lower than the one found (∼5 W) for many continuous high-class GNSS receivers. Table 1 compiles the main characteristics of the GNSS receivers used in the current study.

2.2. Software: Flowchart Process

We used a low-cost single-board Raspberry Pi computer (https://www.raspberrypi.com/ (accessed on 10 January 2024)) to control the Septentrio Mosaic-X5, to manage the data flow and to handle data transmission (Figure 2). The Raspberry Pi was equipped with a 16 GB SD flash memory split into two logical partitions. The first partition hosts the Linux Raspbian operating system and uses an Overlay File System that prevents corrupting the integrity of the SD memory. It also ensures that the system always reboots in the same user-defined configuration. The second partition is dedicated to the data management.

We developed software that manages the communication, acquisition, and data storage in the manufacturer's raw format (Septentrio Binary Format, SBF) and the standard international GNSS format (Receiver INdependent EXchange format, RINEX). Internal communication between MOSAIC-HAT and Raspberry PI relies on a point-to-point IP link (P2P, Figure 2) through the serial port at 2 KB/s (kilobytes per second) for a 1-s GNSS sampling rate. Hourly raw files are firstly stored on Raspberry's RAM to reduce the writing cycles in the SD flash card, while a second routine makes a data flush from the RAM to the SD card. A key feature of our Cost-Efficient Multi-GNSS station is the implementation of dedicated routines to convert, compress, and archive GNSS data in raw and RINEX 3 formats using the RTKLIB-convbin tool (https://github.com/rtklibexplorer/RTKLIB (accessed on 10 January 2024)). Hourly raw files are locally archived and then decimated to a single daily file of 24 h at a 30-s sampling rate in the RINEX format. Typical data size is ∼7.5 Megabytes (MB) for an hourly raw file of GNSS observations and ∼2 MB for the RINEX file. Both hourly and daily files are then sent and archived to a data center through an open VPN connection. We also included a ring buffer script that cyclically deletes the oldest data from the SD memory. In parallel, real-time observation streaming uses the standard Ntrip protocol (Figure 2).

The Raspberry is connected to the internet through a 4G USB cellular modem. The modem is automatically restarted in case of connection loss. The Raspberry is configured as a router in order to enable (1) direct access to the GNSS receiver settings from outside (2) to allow communication from the GNSS receiver to the Ntrip caster when selecting the real-time stream option, (3) to monitor the status of the station, and (4) to allow bidirectional data transmission (Raspberry - external server) based on the rsync incremental backup tool. We make all the developed routines and software publicly available on Gitlab (https://gitlab.com/maurinv/septentrio_mosaic_receiver (accessed on 6 March 2024)).

3. Results

We assess the performance of our all-in-one low-cost GNSS station, hereafter referred to by code SEPT, against existing nearby or co-located equipment. Compared stations are: (1) the SimpleRTK2B electronic board (https://www.ardusimple.com/product/simplertk2b/ (accessed on 10 January 2024)), also manufactured by Ardusimple. Such a board integrates the Ublox's ZED-F9P GNSS module (https://www.u-blox.com/en/product/zed-f9p-module (accessed on 10 January 2024)) and does not track all available GNSS signals (Table 1). We used the same approach described above to control the SimpleRTK2 board and its data flow using a Raspberry PI card. The u-blox receiver is, hereafter, referred to as code UBLO. The Septentrio Mosaic-X5 and Ublox ZED-F9P GNSS receivers are both connected to an Ardusimple AS-ANT3BCAL antenna (https://www.ardusimple.com/product/calibrated-survey-gnss-quadband-antenna-ip67/ (accessed on 10 January 2024)) using a GNSS antenna splitter (https://www.instockwireless.com/gps-antenna-signal-splitter-gps220.htm(accessed on 10 January 2024)). (2) Site SOPH, equipped with a Trimble NetR9 receiver and Ashtech Choke ring antenna, located a few meters away from the SEPT and UBLO sites. (3) Site NICE is located 20 km away from SEPT, UBLO and SOPH, equipped with a Trimble NetR9 receiver and Zephyr 2 antenna. SOPH and NICE are part of the National French GNSS Network (RENAG, http://renag.resif.fr/fr/ (accessed on 6 March 2024)) and hence continuously record GNSS data [15] analyzed by numerous analysis centers (IGS, EUREF, NGL, Renag, etc.). They show typical long-term repeatabilities of 0.1 and 0.3 mm/yr over 22 years of observations, for the horizontal and vertical components, respectively [16].

In the following, we first evaluate the satellite data tracking performance for each system. Then we compare the results obtained for static positioning and finally show the results obtained for kinematic positioning.

3.1. Data Statistics and Quality

The statistical analysis of recorded data directly provides a first evaluation of the performance of our low-cost GNSS SEPT station. Such analysis provides qualitative information that reflects (1) the performance of the receiver tracking throughout time and (2) the level of multipath error and cycle slips from environmental conditions (e.g., buildings, trees, etc.) that could affect positioning accuracy. Statistics computed with the Anubis software (ver 3.7 [17]) show that satellite tracking capacities (Figure 3) and the number of daily GNSS observations above the horizon from the SEPT, SOPH, and NICE stations are consistent (75–85%) during the evaluated time interval (from June 2022 to July 2023). However, the number of observations at the UBLO station is ∼20% lower than SEPT and SOPH for most days since April 2023, a result consistent with [13]. On the other hand, we also observe lower daily cycle slip values at the SEPT station relative to those observed at the low-cost UBLO station for all GNSS constellations (Figure 4), suggesting a higher signal-to-noise ratio and probably less drifting in the receiver's clock. Additionally, cycle slips at SEPT are consistent with values at the permanent NICE station for the GPS, Galileo and BeiDou constellations and at the SOPH station for the GPS constellation. For the GLONASS constellation, the cycle slips are slightly higher at SEPT than NICE and SOPH.

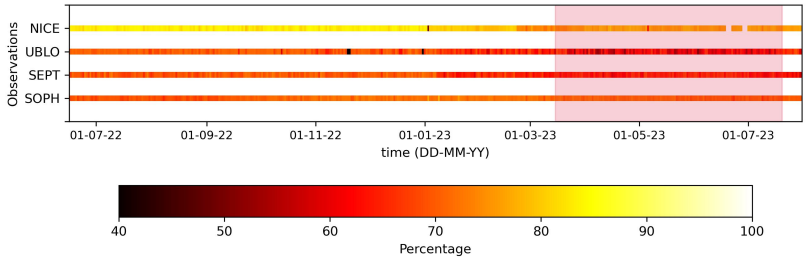

Figure 3. Satellite tracking evaluation regarding the number of daily GNSS observations above the horizon retrieved by the SEPT, UBLO, SOPH, and NICE stations. The light pink vertical stripe depicts the time interval where, for most days, GNSS observations of the UBLO station decrease by ∼20%.

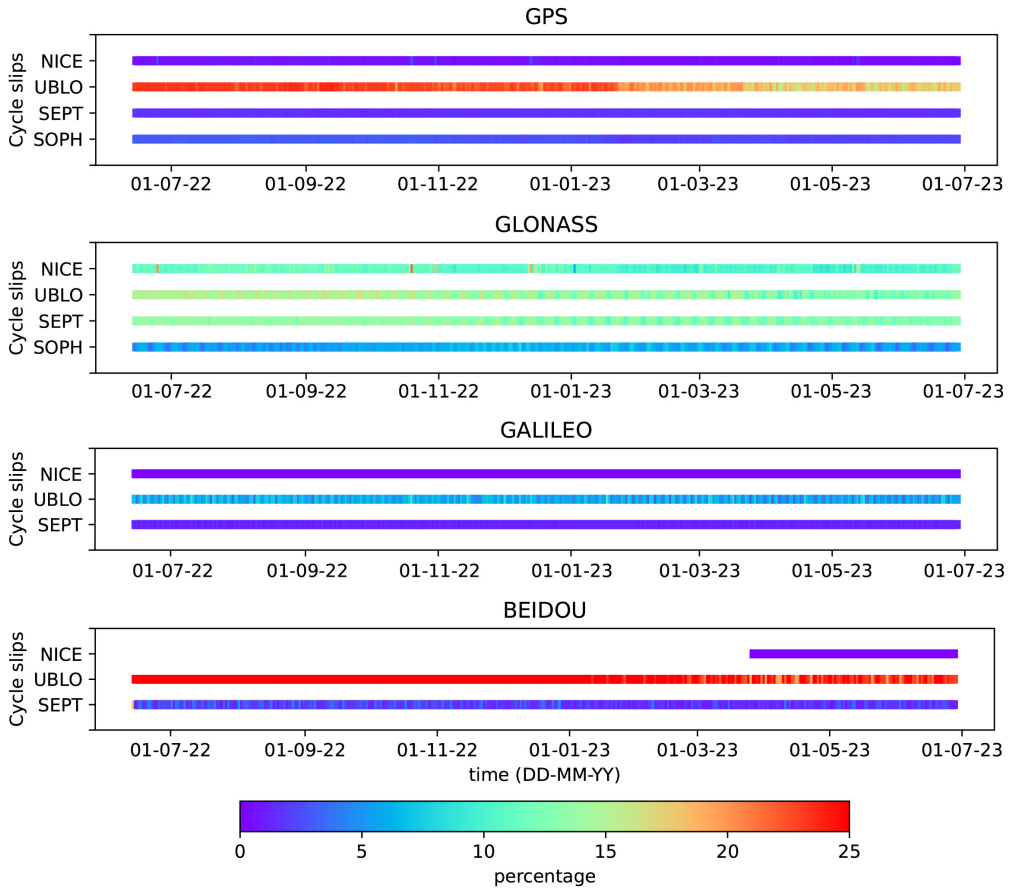

Figure 4. Daily cycle slip values estimated at the SEPT, UBLO, and SOPH sites for the GPS and GLONASS constellations (SEPT and UBLO shared antenna is 5 m apart from SOPH antenna, Table 1). In order to assess the quality of the low-cost stations for the Galileo and BeiDou constellations, we have also included the NICE station, located 20 km away, in the comparison. BeiDou GNSS observations on the NICE site started after the last receiver replacement in March 2023.

Aside from the results of cycle slips described above, Figure 5 depicts an example of the multipath error estimation for the SEPT, UBLO, SOPH, and NICE stations on the L2 frequency (GPS, GLONASS) and for NICE, SEPT, and UBLO on L7 (Galileo, BeiDou). Since the environment surrounding the antenna of the NICE station is slightly different from the others, we have included it in the comparison to have first-order information in the statistics for the Galileo and BeiDou constellations. The comparison, therefore, shows lower multipath values at the SEPT station (∼30 cm for GPS-GLONASS and ∼2 cm for Galileo) relative to the UBLO station (40–45 cm for GPS-GLONASS and ∼26 cm for Galileo) for all constellations, suggesting an excellent algorithm of multipath mitigation that might also

result in lower noise levels at the positioning solution. Surprisingly, multipath values at SEPT are also quite similar or even lower than values observed at the SOPH station, pointing out the excellent accuracy of the low-cost antenna as suggested in Krietemeyer et al. [18] and Curone et al. [12].

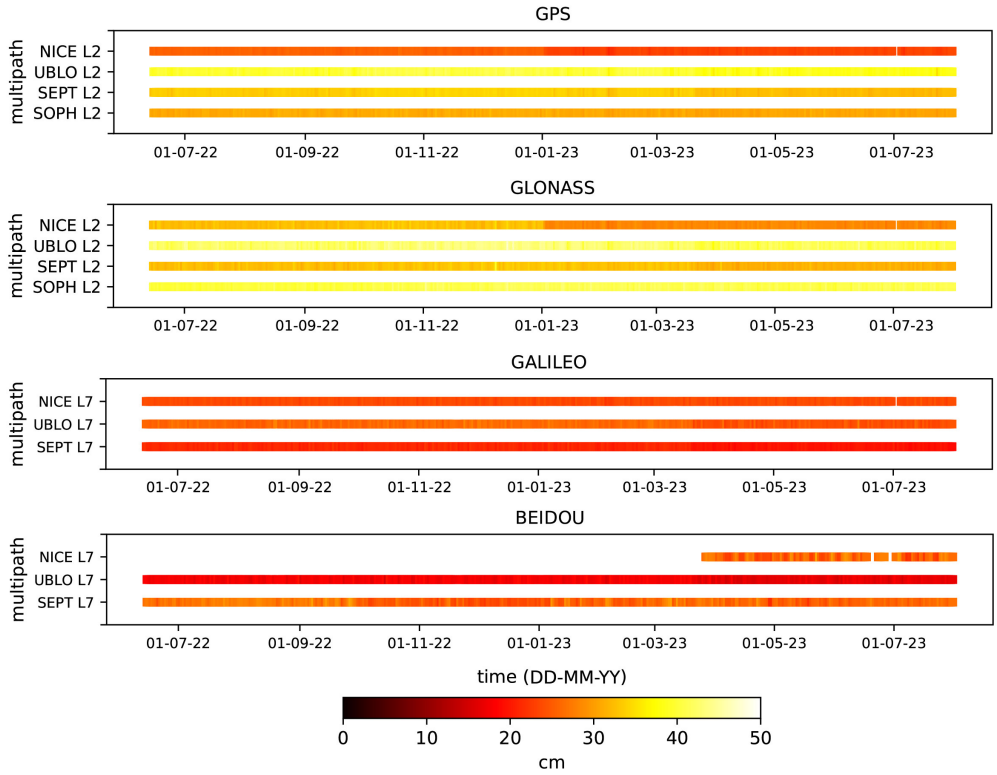

Figure 5. Daily multipath error computed for the L2 (GPS and GLONASS) and L7 (Galileo) frequencies at the SEPT, UBLO, and SOPH stations. In order to assess the quality of the Low-cost sites for the Galileo and BeiDou constellations, we have included the NICE station in the comparison. BeiDou GNSS observations on the NICE site started after the last receiver upgrade in March 2023. Multipath values are in centimeters.

3.2. GNSS Positioning—Daily Solution

Geophysical disciplines, such as seismology or geodesy, are focused on characterizing as accurately as possible short and long-term processes linked to tectonic plate motions and other Earth's internal deformation processes (loading, fluids, etc.). From the point of view of geodynamics, for example, continuous GPS measurements provide direct information to quantify the surface displacement related to the different phases of the seismic cycle (inter-cos-pos-seismic, episodic and transient slow slip events) and model the potential processes that generate them (e.g., [1,19,20]). Hence, we analyze GNSS observations from the low-cost stations at a 30-second sampling rate to assess their consistency relative to high-class GNSS stations by recording the crustal motion in nearby or co-located sites over a year.

Daily GNSS observations were analyzed in sessions of 24 h using the Gamit/Globk software (release 10.71), following the two-step classical MIT approach for geodynamics [21,22]. In the first step, we used a network of 30 well-distributed GNSS sites in France and neighboring areas to produce daily loosely constrained solutions per constellation (GPS, GLONASS, and Galileo) by reducing double-differences of phase to coordinates. At this step, we follow, in general, International GNSS Service (IGS) standards to model elastic effects due to ocean, polar, and solid-earth tides. We used IGS tables to account for phase center variations of antennas and the Vienna Mapping Function (VMF1 [23]) to model the delay of the GNSS signal crossing the troposphere. We refer readers to Jarrin et al. [24]

for a more detailed description of the Gamit processing procedure. Final combined orbits from the International GNSS service were used to process the GPS constellation and the GNSS combined 1-day orbits (MGEX) for GLONASS and Galileo [25,26]. In the second step, we express our solution with respect to the cumulative up-to-date solution from the global IGS-GNSS network by applying a 7-parameters Helmert transformation to produce position time series in the International Terrestrial Reference Frame (ITRF14) [27] for the GPS (G), GLONASS (R), Galileo (E) constellations, and multi-constellations (GR, GE, GER).

We firstly observe a good agreement in the time series trend—at all components in the ITRF reference frame—recorded for the low-cost SEPT and UBLO stations relative to the SOPH and NICE high-class stations (Supplementary Materials Figure S1). Figure 6 shows the detrended time series for the GPS constellation at the NICE, SOPH, SEPT, and UBLO stations. The visual comparison, in general, highlights a good consistency of residual positions for the three components (NEU) at the SEPT and UBLO stations relative to SOPH and NICE, supporting the performance of the low-cost equipment. In detail, however, we can notice that several residual positions depart a few millimeters at all components of UBLO, suggesting a little increase in noise content. A similar behavior is also observed when comparing residuals from the UBLO time series for the GLONASS constellation (Supplementary Materials Figure S2). To better illustrate that, we computed the daily repeatability of residual positions, which is an indicator of the precision, defined as the weighted residual mean squared (WRMS) of daily positions (Equation (A1) in Appendix A [28]). Short-term repeatabilities (GPS solution) computed over 1.1 years are ∼1.5 mm for the horizontal components and 3–4 mm for the vertical component of the SOPH, NICE, and SEPT stations (Figure 7). However, short-term repeatabilities for UBLO are 0.5–1 mm higher than those estimated for the other stations in the north and vertical components. Regarding the GLONASS solution, repeatabilities increase by ∼0.5 mm for the horizontal components, likely suggesting a decrease in the precision of the GLONASS solution. Unfortunately, the L7 (E5b) frequency tracked by the Ublox receiver is not recognized by Gamit/Globk, the repeatabilities for the Galileo solution can only be evaluated at SEPT and NICE. A similar drawback in the Galileo observations was obtained while we analyzed data from the Ublox receiver using the precise point positioning approach from the GINS software (ver 22 [29,30]). Therefore, repeatabilities for the Galileo solution at SEPT and NICE are compatible with the estimated values for the GPS solution. In the case of multi-GNSS solutions (GR, GE, GRE), repeatability values do not indicate an improvement of the precision at the horizontal components, but do for the vertical component (∼0.5–1 mm/yr), relative to the values of the GPS constellation. WRMS values are available in the Supplementary Information (Table S1).

In addition to the repeatability, we also evaluated the noise property of the residual time series for the GPS, GLONASS, and Galileo solutions by computing the Power Spectral Density (PSD). The PSDs show a flat spectrum at high frequencies and a slope of roughly -1 at low frequencies for all sites (Figure 8), consistent with a white and flicker noise combination, as is observed in regional or global GNSS stations. We also notice that power is slightly higher at high frequencies for the UBLO station (∼0.2–0.5 mm^2/cycles per year) relative to the other stations (GPS and GLONASS spectrums). Interestingly, we also notice that power magnitude, at the east component of all stations, for the GLONASS spectrum increases by above one decade (10^1 mm^2/cycles per year) relative to the power in the GPS and Galileo at all frequencies, which is consistent with the substantial improvement of the GPS and Galileo products in the last years (orbit, clock parameter estimation, etc. [26,31]). Overall, noise magnitudes at our low-cost station (SEPT) are almost identical to the ones at the high-class geodetic stations.

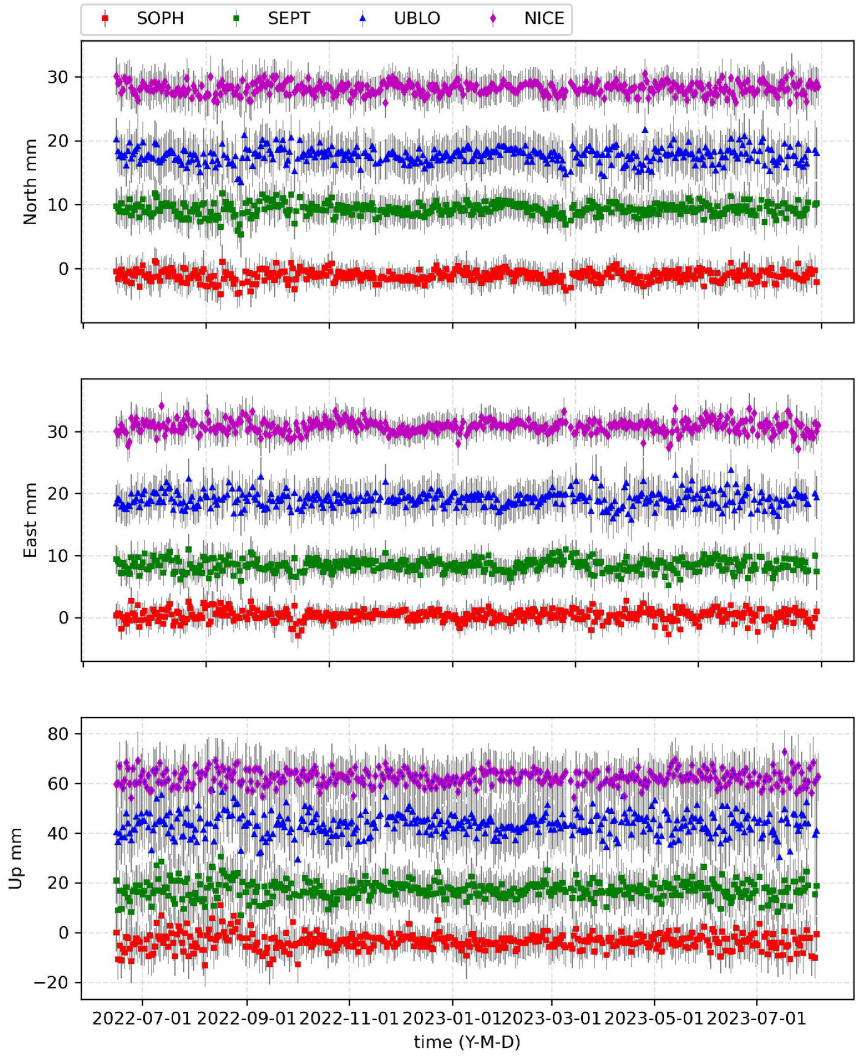

Figure 6. Detrended daily position time-series with associated uncertainties (gray bars) for the SEPT, UBLO, SOPH, and NICE GNSS sites using Gamit-Globk software release 10.71. Time series are, therefore, solutions for the GPS constellation (static mode).

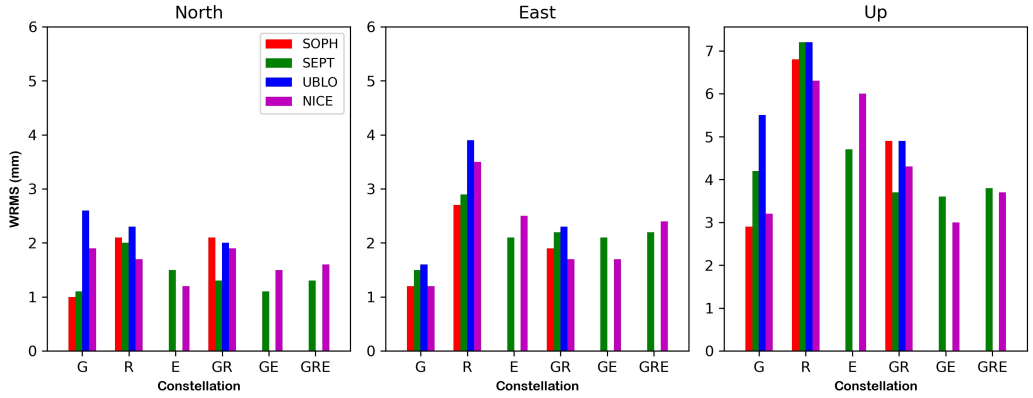

Figure 7. Repeatability (WRMS) computed from daily residual positions for the GNSS processing in the static mode. The x-axis depicts the GNSS solution according to the selected constellation. G: GPS, R: GLONASS, E: Galileo, GR: GPS-GLONASS, GE: GPS-Galileo, GRE: GPS-GLONASS-Galileo.

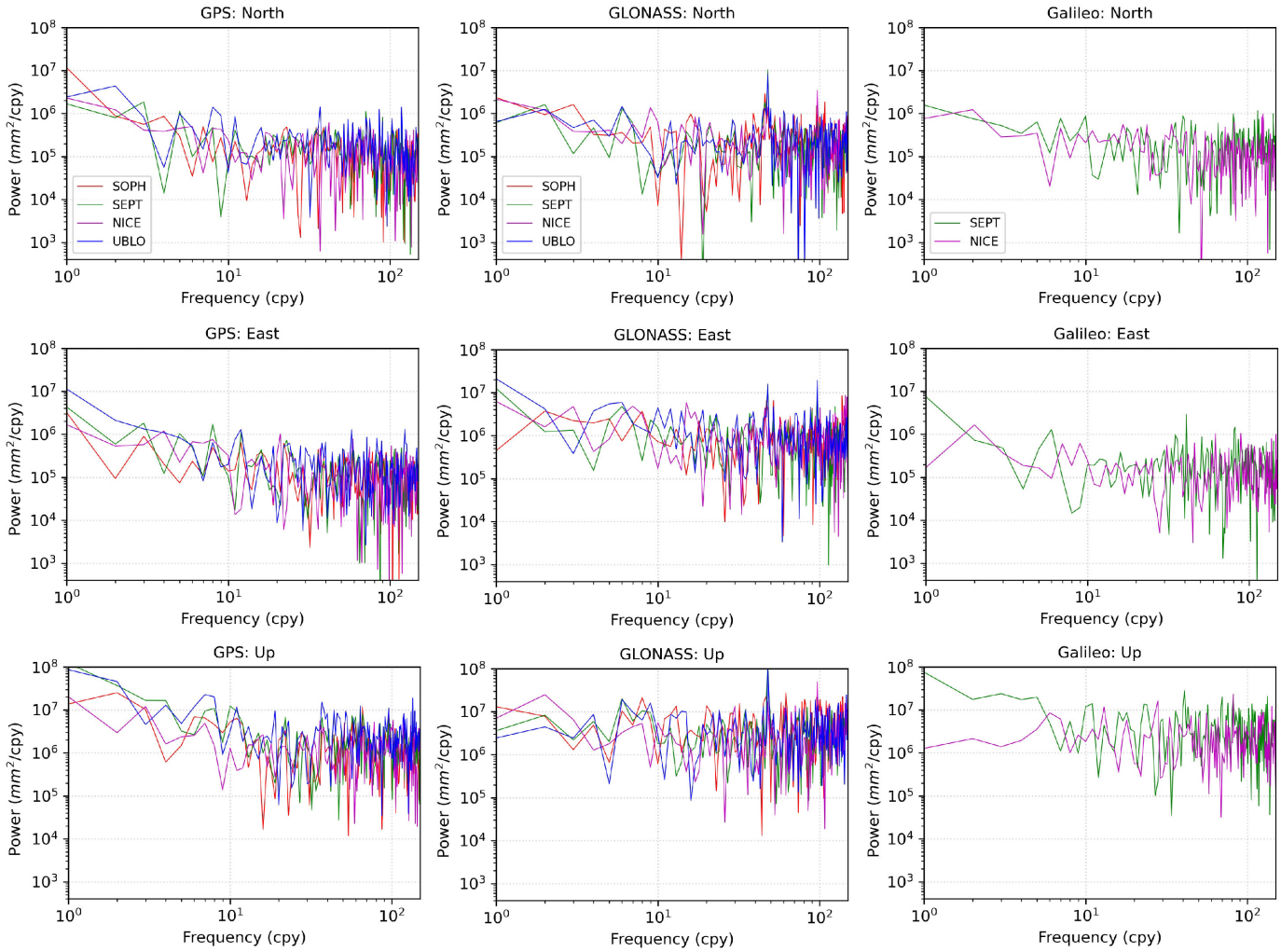

Figure 8. Power Spectral Densities (PSD) for the NICE, SOPH, SEPT and UBLO GNSS sites. PSD are computed for the GPS, GLONASS, and Galileo constellations using the CATS software (ver 3.1.2 [32]). cpy: cycles per year.

3.3. GNSS Positioning—Kinematic Solution

Aside from the static positioning discussed above, geodetic positioning also provides meaningful information on the surface displacement kinematics during an earthquake. Several studies have shown that the inversion of high-rate kinematic displacements, together with other data sets from static GPS displacements, accelerometer, interferometric synthetic aperture radar (InSAR), and global broadband seismometer, allows obtaining a high-quality spatio-temporal image of the seismic rupture kinematics on the subduction interface following large thrust earthquakes (e.g., [2,33,34]). High-rate GNSS time series have also recently been used to image the early postseismic phase, i.e., the deformation that follows the earthquake just after the seismic waves stop (after a few minutes) (e.g., [35,36]). In order to assess the ability of our low-cost SEPT station to record kinematic displacements, we performed a kinematic solution using the precise point positioning approach embedded in the GINS software(ver 22 [29,30]). Similarly to the Gamit/Globk setup, we used final products (orbits, clock offsets) and input models (e.g., Ocean tide loading correction) following the IGS and CNES (Centre National d'Études Spatiales) recommendations, as described in Chupin et al. [37].

Figure 9 shows an example of the kinematic displacements estimated for the GPS constellation at a 1-s sampling rate on the NICE, SEPT, SOPH, and UBLO stations on 23 July 2023. The visual comparison indicates a similar displacement evolution on SOPH,

SEPT, and NICE for all components (Figure 9). As expected, their accuracy (repeatabilities) reaches values at the centimeter level, ∼2 cm for the horizontal components and ∼3 cm for the vertical, with similar noise levels for all frequencies. On the contrary, the UBLO station shows recurrent gaps and steps in its displacement evolution, pointing to a temporal loss in the receiver satellite tracking capacities (Figure 9G) that could not be overcome by adding a second constellation in the analysis (e.g., multi-GNSS solution, Figure 10). Regarding the noise content, we notice the UBLO station is noisier than the other evaluated stations at low frequencies (power spectral densities in Figure 9D–F), which is consistent with the increase in their repeatability values at 3–4 cm/day for both horizontal and vertical components. To obtain better statistics in evaluating the kinematic displacements, we randomly selected 12 days (1 day per month) covering the same time interval, 1.1 year-long, as for the static daily solutions discussed above. On each selected day, we performed a kinematic solution at a 1-s sampling rate and estimated their repeatability (WRMS).

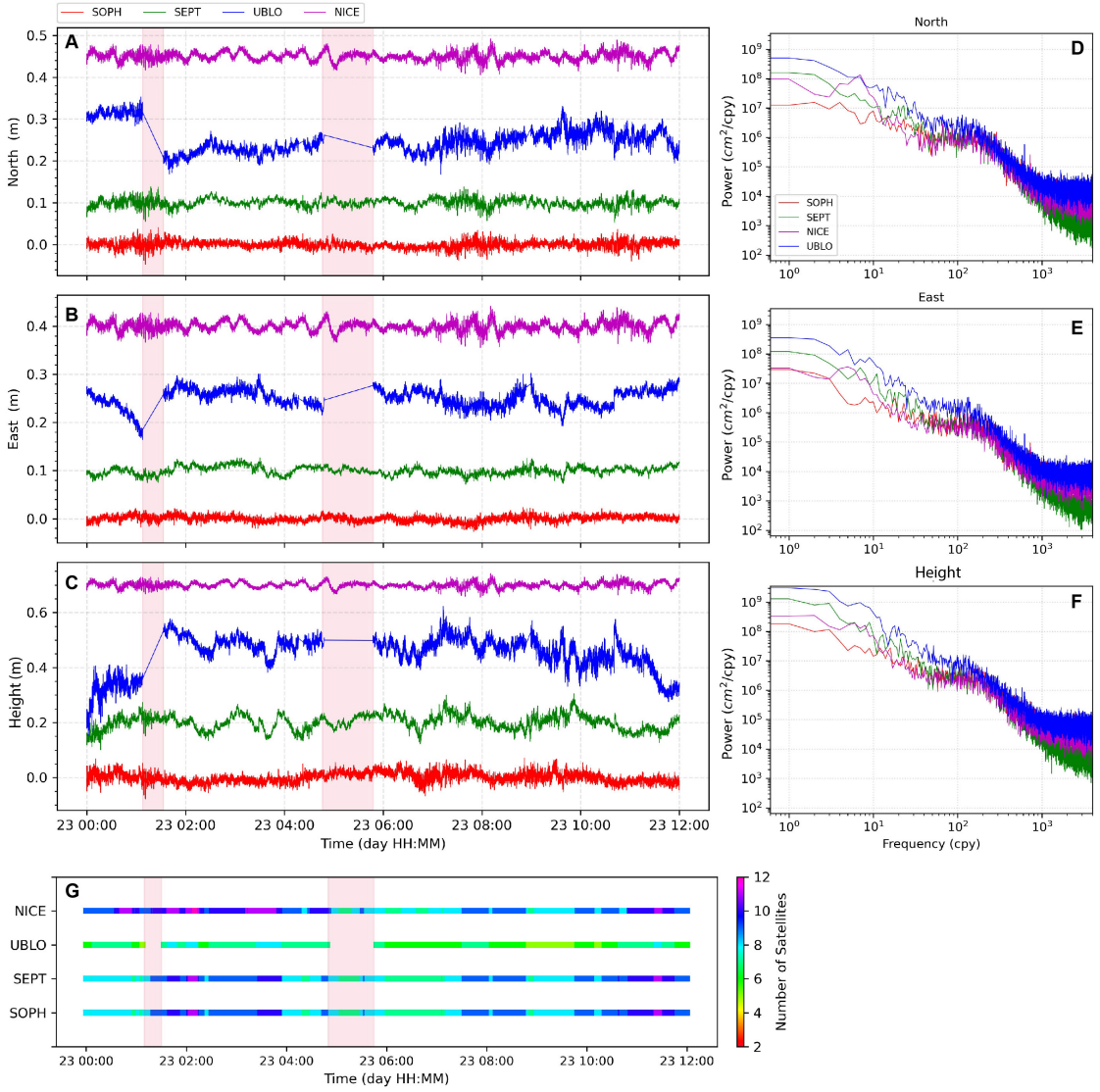

Figure 9. Kinematic displacement for the 1-s sampling rate at the NICE, SEPT, SOPH, and UBLO sites on 23 July 2023. (**A**–**C**) panels depict the kinematic displacements for the GPS constellation. Detrended traces have been shifted to avoid overlap. Light pink vertical stripes within the left panels indicate the displacement gaps at the UBLO site. (**D**–**F**) are the power spectral densities (PSD) estimated from the detrended kinematic displacements at NICE, SEPT, SOPH, and UBLO. (**G**) Number of available satellites tracked by geodetic receivers from GPS observations at a 1-s sampling rate.

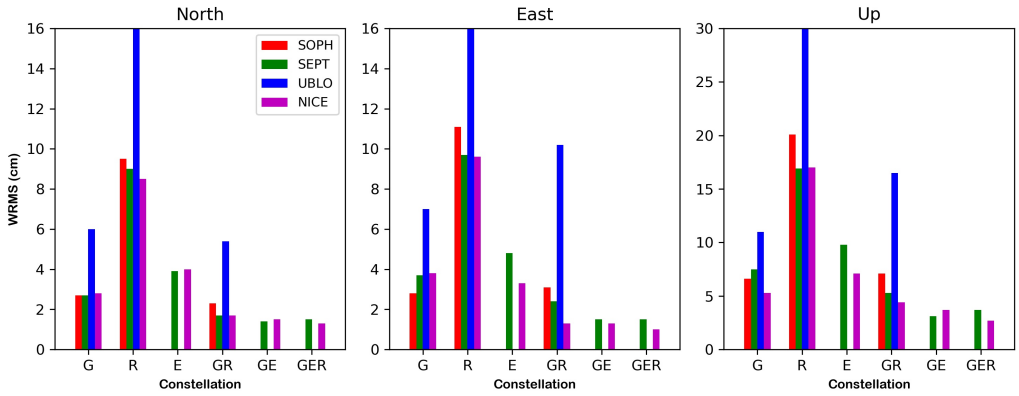

Figure 10. Repeatability (WRMS) computed from residual positions randomly selected (1 day per month) for the GNSS kinematic processing. The x-axis depicts the GNSS solution according to the selected constellation. G: GPS, R: GLONASS, E: Galileo, GR: GPS-GLONASS, GE:GPS-Galileo, GRE: GPS-GLONASS-Galileo.

The histograms in Figure 10 display the average WRMS value from the 12-day kinematic solutions. We observe large WRMS for the UBLO station, which increase by ∼50% (∼3 cm) at all components (NEU) relative to those computed on SEPT and SOPH for the GPS (G) and GPS-GLONASS multi-GNSS (GR) solutions. Additionally, we found abnormal displacements with recurrent gaps on the kinematic solution of the UBLO station for the GLONASS constellation, promoting unrealistic WRMS values (∼1 m). This was also the case when we evaluated UBLO's kinematic solution for GLONASS by using the Track/Gamit software (release 10.71 [21,22]). We, therefore, exclude them from our comparison in order to avoid biasing the statistics. As expected, repeatability values at SEPT are quite similar to NICE (e.g., ∼3 and 7 cm/yr for the horizontal and vertical components for the GPS solution) and in specific cases slightly lower (GLONASS solution) than values at SOPH, supporting the accuracy and reliability of our low-cost station for both the horizontal and vertical components. Contrary to the daily position solution, WRMS estimates from multi-GNSS solutions (GR, GE, GRE) suggest an improvement in the accuracy of the kinematic solution for both the horizontal (∼1 cm) and vertical (decrease ∼2–3 cm/yr) components of the NICE and SEPT stations.

3.4. GNSS Positioning—Real Time Solution

In the last years, real-time GNSS analysis has shown significant progress and contributions to crustal deformation studies and other real-time applications (volcano monitoring, meteorology, etc.). These advances have made it possible to include real-time GNSS displacements at a 1-s sampling rate (1 Hz) in tsunami prediction models and earthquake early warning systems [1,38]. As the last evaluation of the low-cost SEPT station, we performed a real-time multi-GNSS (GPS, GLONASS, Galileo, Beidou) solution during one month of data at high frequencies (1 Hz) using the PPP approach from the BKG client software (ver 2.12.18 [39]). Our data analysis included real-time product streams (orbits and clocks) supported by the IGS through the CDDIS holding (Crustal Dynamics Data Information System).

Figure 11 shows real-time displacements at the NICE, SEPT, SOPH, and UBLO stations on 27 September 2023. At first glance, we notice a poorer performance of the UBLO station, which is consistent with their data quality statistics (multipath error, cycle slip, Figures 4 and 5) and the noise level discussed in the previous sections (Figure 8). Furthermore, the UBLO station also shows several gaps, steps and recurrent departs (spikes up to ∼20 and ∼100 m in the horizontal and vertical components, respectively) from its average displacement at all components of the time series, which is not related to missing real-time products but points to a non-stable satellite tracking performance at several epochs (loss of satellite signals, Figure 11D). Such behavior in the displacement solution at UBLO is recurrent throughout the whole evaluated time interval (from September to

October 2023), causing a fake detection of displacements that could introduce significant bias in the case of computing peak ground displacements (PGD) to be included in fast near-real-time earthquake magnitude determination. Similar to the kinematic and static solutions in post-processing mode, the BKG software (ver 2.12.18) did not recognize Galileo observations tracked on the UBLO receiver, which seems to decrease its accuracy for real-time positioning.

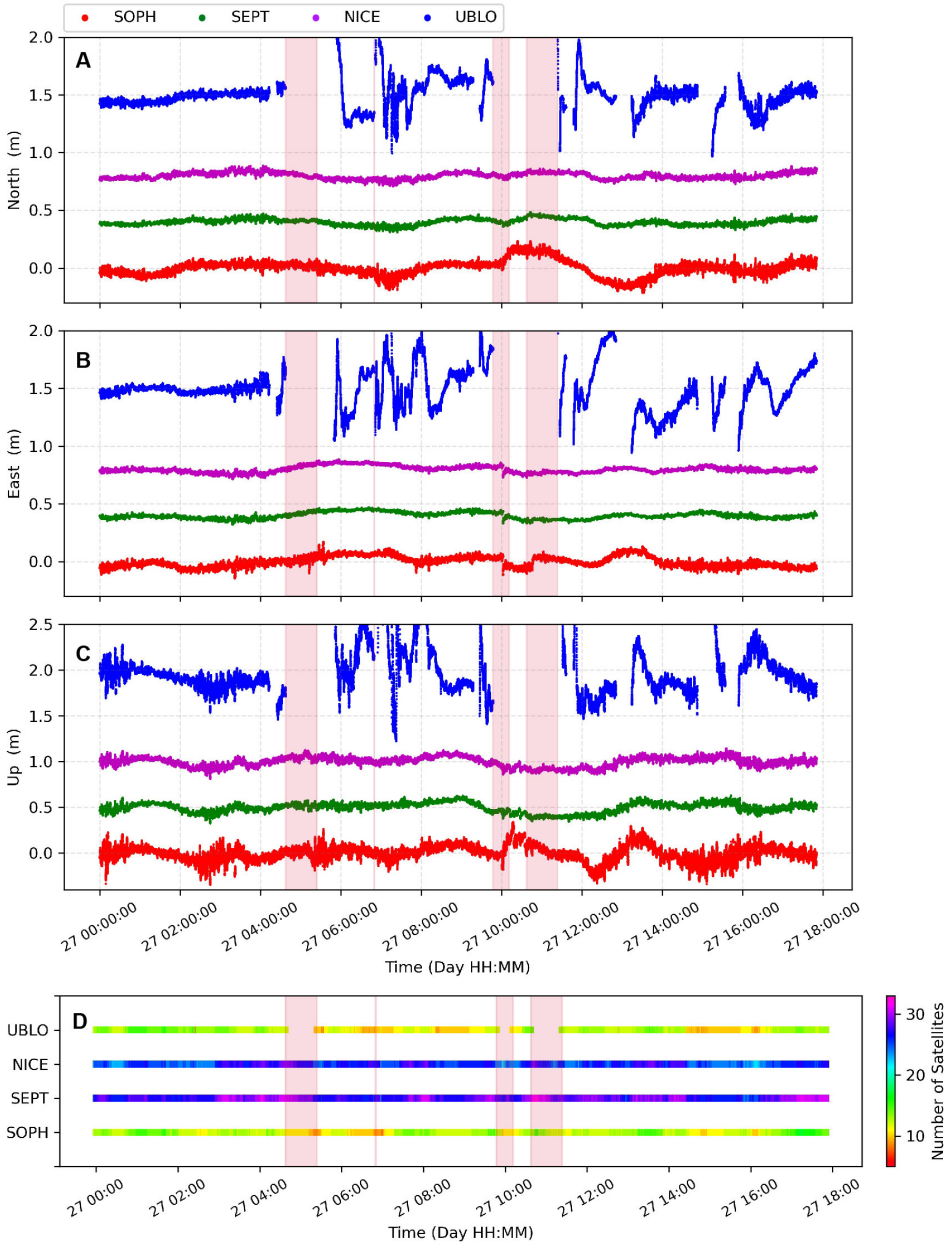

Figure 11. Kinematic displacements from the real-time analysis at the SOPH, SEPT, NICE, and UBLO stations for the North (**A**), East (**B**), and Vertical (**C**) components on 27 September 2023. (**D**) Number of available satellites tracked by geodetic receivers from GNSS observations at a 1-s sampling rate. For visualization purposes, displacements greater than 0.8 m in the UBLO solution are not shown in the comparison. Light pink vertical stripes depict gaps in the kinematic solution and the loss of satellite tracking capacities of the UBLO receiver.

On the contrary, our low-cost SEPT station surprisingly reaches a similar level of accuracy in all components if we compare them with respect to the NICE and SOPH high-class stations. Indeed, repeatability values at SEPT and NICE are ∼3 and ∼5 cm for the

horizontal and vertical components and ∼4 and ∼7 cm estimated at SOPH for the same components. Repetabilities are, therefore, in the range expected for real-time solutions, as proposed in other studies (e.g., Hohensinn et al. [10]).

4. Discussion

Data analysis using different approaches supports the stability and performance of the low-cost SEPT station. The official AS-ANT3BCAL antenna calibration and the noisy mitigation ability of the Mosaic-X5 receiver allow us to obtain daily static or kinematic solutions with the same order of accuracy as the ones estimated by the high-class NICE and SOPH stations. Indeed, short-term repeatabilities from the daily static solution are ∼1 and ∼4 mm for the horizontal and vertical components at SEPT, GPS constellation solution, which is compatible with the long-term repeatability values reported in local and regional continuous high-class GNSS networks. On the contrary, although the low-cost UBLO station (u-blox ZED-F9P receiver) shows repeatability values a little higher than those at NICE, SEPT, and SOPH for the daily static solution (GPS or GLONASS), the north and vertical components of their time series (Figure 6) undergo an increase in noise after few months of continuous recording. This pattern is also evidenced by the slight increase in power magnitudes in the power spectral density plots of Figure 8. The study of Tunini et al. [13], based on daily position solutions for a time window of ∼5 months, reported a few mm accuracy decrease at all position components (NEU) for the u-blox ZED-F9P receiver relative to the accuracy retrieved in the Topcom and Leica high-class receivers. A similar result is also observed in Hanza et al. [11] in which daily position solutions at the same geodetic marker indicated ∼5 mm differences between the u-blox ZED-F9P receiver and the high-class Leica receiver. Our results for the u-blox ZED-F9P (UBLO) are, therefore, in agreement with previous findings.

Regarding the kinematic solutions in post-processing or real-time mode, repeatability values from the low-cost SEPT station are consistent with those computed for the high-class NICE and SOPH stations, supporting the robustness and stability of our GNSS prototype. Interestingly, the average accuracy retrieved at SEPT in real-time mode is ∼3 and ∼5 cm for the horizontal and vertical components, respectively. Such values are around one order of magnitude higher than those computed for its kinematic solution in post-processing mode (∼2 and ∼3 cm for the horizontal and vertical components) for a multi-GNSS solution (GER). This comparison, together with the results of static positioning, points to the low-cost SEPT station as a reliable instrument with the ability to record signals coming from surface deformation processes linked to slow slip events, volcanic unrest, landslides, etc. On the contrary, we identified some additional drawbacks in the performance of the UBLO station (u-blox ZED-F9P) when we were performing the data processing either in kinematic or static mode. The first constraint was related to the rejection of solving Galileo measurements by all the scientific software used in the current study. Furthermore, real-time analysis at UBLO frequently reported a decrease or the total loss of satellite tracking capacities for the GLONASS constellation and occasionally for the GPS, which seems to promote larger uncertainties in its real-time positioning solution (Figure 11). Although the kinematic solution for the GPS constellation at UBLO shows acceptable repeatability values relative to the other stations (NICE, SEPT, and SOPH), their GLONASS solution is the worst, as noted in the previous section (Figure 10). Recent studies (e.g., Wielgocka et al. [9], Hohensinn et al. [10], Hamza et al. [11], among others) have highlighted an adequate performance in the accuracy of the kinematic solution for the u-blox receiver. However, most of them reported a further degradation in the positioning accuracy for the kinematic or real-time modes (>10 cm) even when their evaluations came from reduced short time windows (a few hours to a few days). Herein, we demonstrate the low-cost SEPT station largely improves the positioning accuracy retrieved by the low-cost UBLO station, based on continuous GNSS surveying for more than one year, making it suitable and a cost-efficient alternative for applications of long-term crustal deformation monitoring or offshore tsunami monitoring using commercial shipping fleets [40].

Turning our attention to hardware design, we notice that Septentrio's company has recently launched a new Mosaic-X5 GNSS module (mosaic-go, https://www.septentrio.com/en/products/gps/gnss-receiver-modules/mosaic-go-evaluation-kit (accessed on 1 October 2023)) as part of an evaluation phase. This compact card benefits from, among other features, data writing cycles through an external SD card memory, allowing the raw and RINEX data access directly at the same GNSS receiver. In addition, Ardusimple also offers a Septentrio Mosaic-X5 board (SimpleRTK3B, https://www.ardusimple.com/product/simplertk3b-x5/ (accessed on 1 October 2023)) with an ethernet extension (https://www.ardusimple.com/product/shield-for-native-ethernet/ (accessed on 1 October 2023)) which offers push-FTP capabilities. Therefore, new products will simplify our original low-cost station design by excluding the Raspberry card, which also means a power consumption reduction. We are currently testing the performance of such a new low-cost GNSS receiver, and we expect to have similar results as those obtained for the SEPT station.

5. Conclusions

We assessed the accuracy and performance of an improved low-cost station (SEPT) by analyzing recorded GNSS measurements such as those performed for the scientific community at high-class geodetic networks. Our results, therefore, support the low-cost station as a reliable instrument with the potential to be used to complement and obtain redundancy in the continuous surveying of slow motions resulting from volcanic deformation, crustal deformation, or tsunami monitoring where conventional high-class geodetic networks are sparse or difficult to maintain. Indeed, we have started deploying several low-cost stations in northern Peru and central Ecuador to improve GNSS surveying of the long-term deformation associated with the subduction process. Our cost-efficient geodetic station integrates a dual frequency mosaic-X5 GNSS receiver, AS-ANT3BCAL antenna, raspberry card, and cellular modem. All-in-one, it can acquire satellite signals from the multi-GNSS constellation and transmit them for post- and real-time processing with a low power consumption ($\sim$3.5 W).

Daily static and kinematic positioning coming from the low-cost SEPT station show short-term repeatability values, over $\sim$1 year, quite similar to those obtained from the high-class geodetic stations (NICE and SOPH), supporting the accuracy and stability of the position solution of our proposed GNSS station. However, large daily position time series will allow us to re-evaluate their long-term accuracy in the forthcoming years, which is not expected to show significant variations. Our results also reveal that the low-cost UBLO station (u-blox F9P) reaches fewer well repeatabilities, the worst for the kinematic and real-time solutions, suggesting a degradation in their accuracy over time. Despite that drawback, we think the u-blox F9P module could be an option for applications where millimeter or sub-millimeter accuracy is undesirable.

Daily static positioning solutions in post-processing mode do not clearly show an improvement in accuracy when including a multi-GNSS constellation solution (GPS, GLONASS, Galileo) but it does for the kinematic and real-time processing. Repeatabilities at randomly selected data for the multi-GNSS solutions (GE or GER, Figure 10) suggest an improvement of $\sim$1 cm for the horizontal components and $\sim$2 cm for the vertical. A further re-evaluation of multi-GNSS accuracy solutions, including an array of high-class and low-cost co-located stations, is intended to be conducted in upcoming studies.

Finally, the cost budget required by our low-cost SEPT station is $\sim$50% more expensive than suggested for the UBLO station (u-blox F9P: Table 1) but only $\sim$10% of the price of a high-class geodetic station. Such a budget supports good cost-effectiveness to achieve high positioning solution accuracy.

Supplementary Materials: The following supporting information can be downloaded at: https://www.mdpi.com/article/10.3390/rs16060991/s1, Figure S1: Daily position time series relative to ITRF14 for the NICE, SOPH, SEPT, and UBLO sites. The time series corresponds to the solution of the GPS constellation, estimated with the Gamit & Globk software (ver 10.71); Figure S2: Detrended daily position time series relative to ITRF14 for the NICE, SOPH, SEPT, and UBLO sites. The time

series corresponds to the solution of the GLONASS constellation, estimated with the Gamit & Globk software (ver 10.71); Figure S3: Detrended daily position time series relative to ITRF14 for the NICE and SEPT sites. The time series corresponds to the solution of the Galileo constellation, estimated with the Gamit & Globk software (ver 10.71); Table S1: Summary of residual values from the low-cost and high-class geodetic stations described in the main text and other high-class geodetic stations used to process GNSS observations from Gamit & Globk. The time interval used to estimate wmrs values is over 1.1 years of observations, as described in the main text.

Author Contributions: Conceptualization, P.J., L.R. and M.V. (Maurin Vidal); designed and software M.V. (Maurin Vidal); data curation M.V. (Maurin Vidal), L.R. and P.J.; formal analysis, P.J.; validation, P.J., M.V. (Maurin Vidal), L.R. and J.-M.N.; writing—original draft preparation, P.J., L.R. and M.V. (Maurin Vidal); writing—review and editing, P.J., L.R., M.V. (Maurin Vidal), J.-M.N., M.V. (Mathilde Vergnolle) and P.S. All authors have read and agreed to the submitted version of the manuscript.

Funding: This research received no external funding.

Data Availability Statement: RINEX data are available online through the RENAG GNSS network repository (NICE, SOPH (https://renag.resif.fr/pub/data/ (accessed on 10 January 2024))) and SEPT, UBLO (https://renag.resif.fr/pub/low-cost/SOPH/rinex3_24h_30s/ (accessed on 10 January 2024)). Additional data related to this paper may be requested from the corresponding author. The developed software controlling all functionalities of our low-cost prototype is available on Gitlab (https://gitlab.com/maurinv/septentrio_mosaic_receiver (accessed on 6 March 2024)).

Acknowledgments: We acknowledge support from the Agence Nationale de la Recherche (ANR) in the frame of the ANR-19-CE04-0003 ITEC project, support from the french space agency CNES (APR UV-TEC-GEOX project) and BQR OCA, as well as incentives from RENAG CNRS-INSU SNO and EPOS-France. P. Jarrin's postdoctoral fellowship is funded by the ITEC project. We thank Olivier Laurain for fruitful discussions about the GINS software parameterization. Data are provided by the Research Infrastructure Epos-France (www.epos-france.fr, accessed on 6 February 2024). The network from which this data originates is the Rénag network [15]. They are distributed by the Rénag data center [41]. We thank the Editor and the three anonymous reviewers for thoughtful reviews and comments that improved the paper.

Conflicts of Interest: The authors declare no conflicts of interest.

Appendix A

We use the Weighted Residual Mean Square (*WRMS*) value from the residual time series to assess the accuracy of the position solutions [28].

$$WRMS = \sqrt{\frac{\sum_{i=1}^{n} \frac{(x-\overline{x})^2}{\sigma^2}}{\sum_{i=1}^{n} \frac{1}{\sigma^2}}} \quad \text{(A1)}$$

where n is the number of positions, $\overline{x}$ is the weighted average of the daily positions of x_i or the value predicted by an evolution model, σ_i is the daily position variance of x_i.

References

1. Bock, Y.; Melgar, D. Physical applications of GPS geodesy: A review. *Rep. Prog. Phys.* **2016**, *79*, 106801. [CrossRef] [PubMed]
2. Nocquet, J.M.; Jarrin, P.; Vallée, M.; Mothes, P.A.; Grandin, R.; Rolandone, F.; Delouis, B.; Yepes, H.; Font, Y.; Fuentes, D.; et al. Supercycle at the Ecuadorian subduction zone revealed after the 2016 Pedernales earthquake. *Nat. Geosci.* **2016**, *10*, 145. [CrossRef]
3. Ardusimple on Website. Low-cost GPS/GNSS Products. 2023. Available online: https://www.ardusimple.com/ (accessed on 6 March 2024).
4. Cina, A.; Piras, M. Performance of low-cost GNSS receiver for landslides monitoring: Test and results. *Geomat. Nat. Hazards Risk* **2015**, *6*, 497–514. [CrossRef]
5. Garrido-Carretero, M.S.; de Lacy-Pérez de los Cobos, M.C.; Borque-Arancón, M.J.; Ruiz-Armenteros, A.M.; Moreno-Guerrero, R.; Gil-Cruz, A.J. Low-cost GNSS receiver in RTK positioning under the standard ISO-17123-8: A feasible option in geomatics. *Measurement* **2019**, *137*, 168–178. [CrossRef]

6. Zumberge, J.F.; Heflin, M.B.; Jefferson, D.C.; Watkins, M.M.; Webb, F.H. Precise point positioning for the efficient and robust analysis of GPS data from large networks. *J. Geophys. Res. Solid Earth* **1997**, *102*, 5005–5017. [CrossRef]
7. Zhbankov, G.A.; Danilkin, N.P.; Maltseva, O.A. Influence of the ionosphere on the accuracy of the satellite navigation system. *Acta Astronaut.* **2022**, *190*, 194–201. [CrossRef]
8. Janos, D.; Kuras, P. Evaluation of Low-Cost GNSS Receiver under Demanding Conditions in RTK Network Mode. *Sensors* **2021**, *21*, 5552. [CrossRef]
9. Wielgocka, N.; Hadas, T.; Kaczmarek, A.; Marut, G. Feasibility of Using Low-Cost Dual-Frequency GNSS Receivers for Land Surveying. *Sensors* **2021**, *21*, 1956. [CrossRef]
10. Hohensinn, R.; Stauffer, R.; Glaner, M.F.; Herrera Pinzón, I.D.; Vuadens, E.; Rossi, Y.; Clinton, J.; Rothacher, M. Low-Cost GNSS and Real-Time PPP: Assessing the Precision of the u-blox ZED-F9P for Kinematic Monitoring Applications. *Remote Sens.* **2022**, *14*, 5100. [CrossRef]
11. Hamza, V.; Stopar, B.; Sterle, O.; Pavlovčič-Prešeren, P. A Cost-Effective GNSS Solution for Continuous Monitoring of Landslides. *Remote Sens.* **2023**, *15*, 2287. [CrossRef]
12. Curone, D.; Savarese, G.; Antonini, M.; Baucry, R.; Amani, E.; Boulandet, A.; Cataldo, M.; Chambon, P.; Chersich, M.; Hussein, A.B.; et al. An Innovative Low-Power, Low-Cost, Multi-Constellation Geodetic-Grade Global Navigation Satellite System Reference Station for the Densification of Permanent Networks: The GREAT Project. *Sensors* **2023**, *23*, 6032. [CrossRef] [PubMed]
13. Tunini, L.; Zuliani, D.; Magrin, A. Applicability of Cost-Effective GNSS Sensors for Crustal Deformation Studies. *Sensors* **2022**, *22*, 350. [CrossRef] [PubMed]
14. NOAA US Department of Commerce on Website. Antenna Calibrations on National Geodetic Survey. Available online: https://www.ngs.noaa.gov/ANTCAL/index.xhtml# (accessed on 6 March 2024).
15. RENAG on Website. *Permanent French National Geodetic Network*; Epos-France: Gennevilliers, France, 2023. Available online: http://renag.resif.fr/fr/ (accessed on 6 March 2024).
16. Santamaría, A. *RENAG GNSS Combined Velocity Field [Dataset]*; Epos-France: Gennevilliers, France, 2022.
17. Vaclavovic, P.; Dousa, J. G-Nut/Anubis: Open-Source Tool for Multi-GNSS Data Monitoring with a Multipath Detection for New Signals, Frequencies and Constellations. In *IAG 150 Years*; Rizos, C., Willis, P., Eds.; Springer International Publishing: Cham, Switzerland, 2015; Volume 143, pp. 775–782. [CrossRef]
18. Krietemeyer, A.; van der Marel, H.; van de Giesen, N.; ten Veldhuis, M.C. A Field Calibration Solution to Achieve High-Grade-Level Performance for Low-Cost Dual-Frequency GNSS Receiver and Antennas. *Sensors* **2022**, *22*, 2267. [CrossRef]
19. Blewitt, G.; Hammond, W.; Kreemer, C. Harnessing the GPS Data Explosion for Interdisciplinary Science. *Eos* **2018**, *99*. [CrossRef]
20. Jarrin, P.; Nocquet, J.M.; Rolandone, F.; Audin, L.; Mora-Páez, H.; Alvarado, A.; Mothes, P.; Audemard, F.; Villegas-Lanza, J.C.; Cisneros, D. Continental block motion in the Northern Andes from GPS measurements. *Geophys. J. Int.* **2023**, *235*, 1434–1464. [CrossRef]
21. Herring, T.A.; Floyd, M.A.; King, R.W.; McClusky, S.C. *Global Kalman Filter VLBI and GPS Analysis Program*; Technical Report Release 10.6; MIT: Cambridge, MA, USA, 2015.
22. Herring, T.A.; King, R.W.; Floyd, M.A.; McClusky, S.C. *GPS Analysis*; Technical Report Release 10.7; MIT: Cambridge, MA, USA, 2018.
23. Boehm, J.; Werl, B.; Schuh, H. Troposphere mapping functions for GPS and very long baseline interferometry from European Centre for Medium-Range Weather Forecasts operational analysis data. *J. Geophys. Res. Solid Earth* **2006**, *111*, B02406. [CrossRef]
24. Jarrin, P.; Nocquet, J.M.; Rolandone, F.; Mora-Páez, H.; Mothes, P.; Cisneros, D. Current motion and deformation of the Nazca Plate: New constraints from GPS measurements. *Geophys. J. Int.* **2022**, *232*, 842–863. [CrossRef]
25. Noll, C.E. The crustal dynamics data information system: A resource to support scientific analysis using space geodesy. *Adv. Space Res.* **2010**, *45*, 1421–1440. [CrossRef]
26. Prange, L.; Villiger, A.; Sidorov, D.; Schaer, S.; Beutler, G.; Dach, R.; Jäggi, A. Overview of CODE's MGEX solution with the focus on Galileo. *Adv. Space Res.* **2020**, *66*, 2786–2798. [CrossRef]
27. Altamimi, Z.; Rebischung, P.; Métivier, L.; Collilieux, X. ITRF2014: A new release of the International Terrestrial Reference Frame modeling nonlinear station motions. *J. Geophys. Res. Solid Earth* **2016**, *121*, 6109–6131. [CrossRef]
28. Blewitt, G. Carrier phase ambiguity resolution for the Global Positioning System applied to geodetic baselines up to 2000 km. *J. Geophys. Res. Solid Earth* **1989**, *94*, 10187–10203. [CrossRef]
29. Marty, J.C.; Loyer, S.; Perosanz, F.; Mercier, F.; Bracher, G.; Legrésy, B.; Portier, L.; Capdeville, H.; Lemoine, J.M.; Biancale, R. GINS: The CNES/GRGS GNSS Scientific Software. *ESA Proc.* **2011**, *31*, 8–10.
30. Loyer, S.; Perosanz, F.; Mercier, F.; Capdeville, H.; Marty, J.C. Zero-difference GPS ambiguity resolution at CNES–CLS IGS Analysis Center. *J. Geod.* **2012**, *86*, 991–1003. [CrossRef]
31. Griffiths, J. Combined orbits and clocks from IGS second reprocessing. *J. Geod.* **2019**, *93*, 177–195. [CrossRef]
32. Williams, S.D.P. CATS: GPS coordinate time series analysis software. *GPS Solut.* **2008**, *12*, 147–153. [CrossRef]
33. Delouis, B.; Giardini, D.; Lundgren, P.; Salichon, J. Joint Inversion of InSAR, GPS, Teleseismic, and Strong-Motion Data for the Spatial and Temporal Distribution of Earthquake Slip: Application to the 1999 İzmit Mainshock. *Bull. Seismol. Soc. Am.* **2002**, *92*, 278–299. [CrossRef]

34. Konca, A.O.; Leprince, S.; Avouac, J.P.; Helmberger, D.V. Rupture Process of the 1999 Mw 7.1 Duzce Earthquake from Joint Analysis of SPOT, GPS, InSAR, Strong-Motion, and Teleseismic Data: A Supershear Rupture with Variable Rupture Velocity. *Bull. Seismol. Soc. Am.* **2010**, *100*, 267–288. [CrossRef]
35. Twardzik, C.; Vergnolle, M.; Sladen, A.; Avallone, A. Unravelling the contribution of early postseismic deformation using sub-daily GNSS positioning. *Sci. Rep.* **2019**, *9*, 1775. [CrossRef]
36. Tsang, L.L.; Vergnolle, M.; Twardzik, C.; Sladen, A.; Nocquet, J.M.; Rolandone, F.; Agurto-Detzel, H.; Cavalié, O.; Jarrin, P.; Mothes, P. Imaging rapid early afterslip of the 2016 Pedernales earthquake, Ecuador. *Earth Planet. Sci. Lett.* **2019**, *524*, 115724. [CrossRef]
37. Chupin, C.; Ballu, V.; Testut, L.; Tranchant, Y.T.; Calzas, M.; Poirier, E.; Coulombier, T.; Laurain, O.; Bonnefond, P.; Team FOAM Project. Mapping Sea Surface Height Using New Concepts of Kinematic GNSS Instruments. *Remote Sens.* **2020**, *12*, 2656. [CrossRef]
38. Crowell, B.; Schmidt, D.; Bodin, P.; Vidale, J.; Gomberg, J.S.; Hartog, J.R.; Kress, V.; Melbourne, T.; Santillian, M.; Minson, S.E.; et al. Demonstration of the Cascadia G-FAST geodetic earthquake early warning system for the Nisqually, Washington, earthquake. *Seismol. Res. Lett.* **2016**, *87*, 930–943. [CrossRef]
39. Mervart, L.; Weber, G.; Stürze, A.; Stöcker, D. BKG Ntrip Client—BNC Software. 2023. Federal Agency for Cartography and Geodesy (BKG), Frankfurt, Germany. Available online: https://igs.bkg.bund.de/ntrip/bnc (accessed on 2 May 2023).
40. Foster, J.H.; Brooks, B.A.; Wang, D.; Carter, G.S.; Merrifield, M.A. Improving tsunami warning using commercial ships. *Geophys. Res. Lett.* **2012**, *39*, L09603. [CrossRef]
41. RENAG-DC. Registry of Research Data Repositories. 2022. Available online: https://doi.org/10.17616/R31NJN5L (accessed on 6 March 2024).